JOURNAL OF GUIDANCE, CONTROL, AND DYNAMICS
Vol. 34, No. 3, May–June 2011

Approach Guidance with Double-Line-of-Sight-Measuring Navigation Constraint for Autonomous Rendezvous

Tong Chen* and Shijie Xu†
Beijing University of Aeronautics and Astronautics, 100191 Beijing, People's Republic of China

DOI: 10.2514/1.52963

Based on double-line-of-sight measuring relative navigation method, an approach guidance law with the triangle-measuring constraint is presented for autonomous rendezvous. The observability of double-line-of-sight measuring relative navigation system is analyzed using the state estimation error covariance matrix. The triangle-measuring navigation constraint is described as a keep-out cone. The approach guidance law is designed via artificial potential function method. It is ensured that there is a high region of potential in the keep-out cone and the potential still has a unique minimum at the goal position. Numerical simulations are undertaken to verify the guidance method proposed. The results indicate that the control impulses of the potential function guidance ensure convergence of the chase spacecraft to reach the goal position without violating the navigation keep-out zone.

I. Introduction

TO DATE, there are more and more missions and plans including on-orbit servicing [1–4], asteroid exploration [5], Mars sample return exploration [6], and so on, to address the necessary of space autonomous rendezvous technology. Different from the past space rendezvous operations that often required cooperation between spacecraft and a man-in-the-loop, the notion of performing autonomous rendezvous should satisfy the demand of a variety of rendezvous targets that may be cooperative or uncooperative, functioning or malfunctioning, and passive or active [7,8]. Meanwhile, the complex navigation sensors and guidance instrumentation used for the past rendezvous operations are gradually developed to be with incorporating light weight, low power, and compact configuration. Therefore, the navigation and guidance methods for autonomous rendezvous also face the new challenges to adapt these new characteristics of space autonomous rendezvous. The purpose of this paper is to present an approach guidance method with only line-of-sight (LOS)-angle measurements for autonomous rendezvous.

The angles-only navigation and guidance, sometimes called the stereovision navigation and guidance, is not a new technology and has been exploited in the areas of aeronautic, naval, or other applications [9–11] because of the advantages of requiring only simple vision measuring sensors and LOS-angle measurements. Some research works [12–15] have illuminated that when the relative range between spacecraft is very close (tens of meters) in the final phase of rendezvous and docking, the angles-only navigation is feasible via multi-LOS-vector measurements of several observation beacons mounted on the target spacecraft. However, in the far or medium range (tens of kilometers to several kilometers), operation phase of autonomous rendezvous, the target is merely taken as a point source so that only single-LOS-vector measurements are obtained. Thus many research works have been focused on the navigation problem with only single-LOS measurements available. Chari [16] studied observability of the angles-only navigation system in different orbital rendezvous trajectories both analytically and through linear covariance modeling. Yim et al. [17] investigated the possibility of autonomous orbit navigation using LOS measurements between two orbiting spacecraft with several thousands kilometers distance and determined observability of the navigation system using the condition number of the observability matrix. Woffinden and Geller [18] presented an analytical expression that clearly defines the conditions that ensure observability for a linear navigation system of orbital rendezvous when only LOS-angle measurements are used. Hablani et al. [19–21] also analyzed observability of the relative position from LOS-angle measurements. Chen et al. [22] presented an iterative algorithm to estimate the along-track relative motion using only azimuth angle. Schmidt and Lovell [23] described a method to calculate the geometric aspects of relative satellite motion using angles-only measurements. They all drew the same conclusion that the relative navigation system is weakly observable or even unobservable using only single-LOS-angle measurements in the phases of far- and medium-range rendezvous operations, and the estimation of relative position of the target is gross. For the above reasons, an angles-only relative navigation method—double-LOS-measuring relative navigation has been put forwarded for autonomous rendezvous [24]. It is supposed that two-formation chase spacecraft form a triangle-measuring configuration relative to the target in space so as the observability of the relative navigation system is improved and the relative motion of the target can be estimated precisely. However, the relative navigation system is near unobservable as soon as three spacecraft are in one line. The same conclusion has been obtained by Linares et al. [25]. They determine the relative attitudes of formation vehicles within the close range using the triangle multi-LOS-measuring method.

Based on the previous research work, this paper is focused on the approach guidance law with the triangle-measuring navigation constraint. The purpose of guidance maneuver of the chase spacecraft is not only to approach the target, but also to guarantee the advantage relative motion for the observability of navigation system. Many rendezvous guidance methods have been presented, such as Clohessy–Wiltshire (C-W) two-impulse guidance [26,27], optimal multi-impulse guidance [28,29], impulsive feedback control using classical orbit element differences [30], and so on. However, considering autonomous implementing and navigation constraint, artificial potential function guidance, which was first presented for terminal rendezvous in the presence of path constraints and multiple obstructions by Lopez and McInnes [31], is the most effective method. Thereby, the rendezvous guidance law with navigation constraint will be designed using the artificial potential function method in this paper.

This paper is organized as follows. First, a double-LOS-measuring relative navigation constraint is described. Second, the approach guidance law with navigation constraint is presented. Then two numerical simulation scenarios are undertaken to illustrate the presented guidance method. At last, the conclusion is given.

Received 28 October 2010; revision received 14 December 2010; accepted for publication 16 December 2010. Copyright © 2010 by the American Institute of Aeronautics and Astronautics, Inc. All rights reserved. Copies of this paper may be made for personal or internal use, on condition that the copier pay the $10.00 per-copy fee to the Copyright Clearance Center, Inc., 222 Rosewood Drive, Danvers, MA 01923; include the code 0731-5090/11 and $10.00 in correspondence with the CCC.

*Lecturer, School of Astronautics, Department of Guidance, Navigation and Control; chet@buaa.edu.cn.

†Professor, School of Astronautics, Department of Guidance, Navigation and Control; starsjxu@yahoo.com.cn.

II. Double-LOS-Measuring Relative Navigation Constraint

For noncooperative autonomous rendezvous, double-LOS-measuring relative navigation method has been presented via the notion of human binocular vision [24]. As portrayed in Fig. 1, the architecture of double-LOS-measuring relative navigation comprises a chief chase spacecraft (CCS) that performs maneuver operations to rendezvous with a target spacecraft (TS) and an auxiliary chase spacecraft (ACS). TS is supposed to be passive, disable or noncooperative. CCS and ACS form a measuring baseline relative to the target in space and can transfer the measurement information to each other via the interspacecraft crosslink. CCS and ACS measure relative LOS angles (respectively, azimuth α_i and elevation β_i, $i = 1, 2$) of TS using the optical sensor and acquire their own inertial position/attitude using the inertial measurement instrument, star tracker, and gyro. Meanwhile, the bearing of the measuring baseline (namely, relative LOS angles, azimuth α_b and elevation β_b, of CCS with respect to ACS and the length $\|\Delta\mathbf{r}_b\|$ of the measuring baseline between CCS and ACS) are obtained using interspacecraft measuring. Obviously, if the measuring triangle exists, the range from CCS to TS ($|\Delta\mathbf{r}_1|$ in Fig. 1) and the range from ACS to TS ($|\Delta\mathbf{r}_2|$ in Fig. 1) as well as the relative position of TS can be determined using the above measurements.

The relative navigation model is set up to estimate the relative position and velocity using the filter method. The position vector of TS relative to CCS $\Delta\mathbf{r}_1$ and the position vector of ACS relative to CCS $\Delta\mathbf{r}_b$ are defined as

$$\Delta\mathbf{r}_1 = \mathbf{r}_t - \mathbf{r}_{c1} \tag{1}$$

$$\Delta\mathbf{r}_b = \mathbf{r}_{c2} - \mathbf{r}_{c1} \tag{2}$$

where $\mathbf{r}_t$ is the position vector of TS, and $\mathbf{r}_{c1}$ and $\mathbf{r}_{c2}$ are the position vectors of CCS and ACS, respectively.

When the relative distance between two spacecraft is small in comparison with the absolute orbit radius, the gravity difference can be linearized [32]. The approximate relative-motion equations of TS with respect to CCS and that of ACS with respect to CCS are obtained as

$$\Delta\ddot{\mathbf{r}}_1 = -\frac{\mu}{\|\mathbf{r}_{c1}\|^3}\left[\Delta\mathbf{r}_1 - 3\left(\frac{\mathbf{r}_{c1}^T\Delta\mathbf{r}_1}{\|\mathbf{r}_{c1}\|^2}\right)\mathbf{r}_{c1}\right] + \mathbf{p}(\mathbf{r}_t) - \mathbf{p}(\mathbf{r}_{c1}) - \mathbf{U}_{c1} \tag{3}$$

$$\Delta\ddot{\mathbf{r}}_b = -\frac{\mu}{\|\mathbf{r}_{c1}\|^3}\left[\Delta\mathbf{r}_b - 3\left(\frac{\mathbf{r}_{c1}^T\Delta\mathbf{r}_b}{\|\mathbf{r}_{c1}\|^2}\right)\mathbf{r}_{c1}\right] + \mathbf{p}(\mathbf{r}_{c2}) - \mathbf{p}(\mathbf{r}_{c1}) - \mathbf{U}_{c1} \tag{4}$$

where $\mathbf{p}(*)$ is the perturbation acceleration function of the spacecraft. $\mathbf{U}_{c1}$ is the acceleration of CCS caused by the thrusters for guidance maneuvers. It is supposed that ACS do not perform the rendezvous maneuver and TS is passive. Thereby, they have no orbital control accelerations.

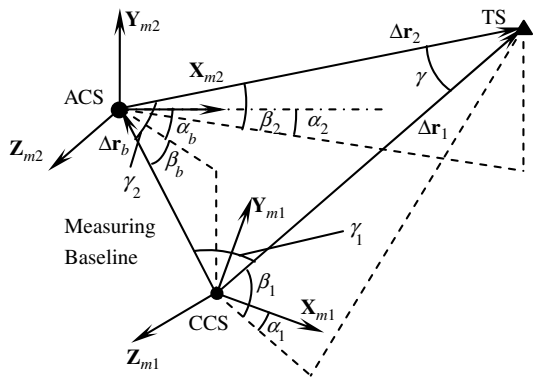

Fig. 1 Relative geometry of double-LOS measurements.

The process noise model is obtained according to the relative-motion equations described in the inertial frame:

$$\dot{\mathbf{X}} = \mathbf{f}(\mathbf{X}) + B\mathbf{U} + D\boldsymbol{\varsigma} \tag{5}$$

where

$$\mathbf{X} = [\,(\Delta\mathbf{r}_1)_i^T \quad (\Delta\dot{\mathbf{r}}_1)_i^T \quad (\Delta\mathbf{r}_b)_i^T \quad (\Delta\dot{\mathbf{r}}_b)_i^T\,]^T$$

$$\mathbf{f}(\mathbf{X}) = \begin{bmatrix} (\Delta\dot{\mathbf{r}}_1)_i \\ \frac{\mu}{\|\mathbf{r}_{c1}\|^3}\left(3\frac{\mathbf{r}_{c1}^T\Delta\mathbf{r}_1}{\|\mathbf{r}_{c1}\|^2}\cdot(\mathbf{r}_{c1})_i - (\Delta\mathbf{r}_1)_i\right) \\ (\Delta\dot{\mathbf{r}}_b)_i \\ \frac{\mu}{\|\mathbf{r}_{c1}\|^3}\left(3\frac{\mathbf{r}_{c1}^T\Delta\mathbf{r}_b}{\|\mathbf{r}_{c1}\|^2}\cdot(\mathbf{r}_{c1})_i - (\Delta\mathbf{r}_b)_i\right) \end{bmatrix},$$

$$\mathbf{B} = \begin{bmatrix} \mathbf{O}_{3\times3} & \mathbf{O}_{3\times3} \\ -\mathbf{I}_{3\times3} & \mathbf{O}_{3\times3} \\ \mathbf{O}_{3\times3} & \mathbf{O}_{3\times3} \\ -\mathbf{I}_{3\times3} & \mathbf{I}_{3\times3} \end{bmatrix}, \qquad \mathbf{D} = \begin{bmatrix} \mathbf{O}_{3\times3} & \mathbf{O}_{3\times3} \\ \mathbf{I}_{3\times3} & \mathbf{O}_{3\times3} \\ \mathbf{O}_{3\times3} & \mathbf{O}_{3\times3} \\ \mathbf{O}_{3\times3} & \mathbf{I}_{3\times3} \end{bmatrix},$$

$$\mathbf{U} = \begin{bmatrix} (\mathbf{U}_{c1})_i \\ (\mathbf{U}_{c2})_i \end{bmatrix}, \qquad \boldsymbol{\varsigma} = \begin{bmatrix} \boldsymbol{\varsigma}_1 \\ \boldsymbol{\varsigma}_2 \end{bmatrix}$$

and where $(*)_i$ represents the column matrix of components of vector in the inertial frame, and $\boldsymbol{\varsigma}_1$ and $\boldsymbol{\varsigma}_b$ are assumed to be white Gaussian process noises that are caused by the differences of the perturbation accelerations of the spacecraft $\mathbf{p}(\mathbf{r}_t) - \mathbf{p}(\mathbf{r}_{c1})$ and $\mathbf{p}(\mathbf{r}_{c2}) - \mathbf{p}(\mathbf{r}_{c1})$. We define the spectral density matrix of process noise $\mathbf{q}$ as follows:

$$\begin{aligned} &E[\boldsymbol{\varsigma}(t)\boldsymbol{\varsigma}(\tau)^T] = \mathbf{q}\delta(t-\tau), \\ &\mathbf{q} = \mathrm{diag}([\sigma_{1x}^2; \sigma_{1y}^2; \sigma_{1z}^2; \sigma_{bx}^2; \sigma_{by}^2; \sigma_{bz}^2]) \end{aligned} \tag{6}$$

where σ_{1x}, σ_{1y}, σ_{1z}, σ_{bx}, σ_{by}, and σ_{bz} are the standard deviations of process noises.

The measurement vector $\mathbf{Z}$ includes LOS angles of TS with respect to CCS α_1 and β_1, LOS angles of TS with respect to ACS α_2 and β_2, LOS angles of CCS with respect to ACS α_b and β_b, and the range between CCS and ACS $\|\Delta\mathbf{r}_b\|$. The measurement model is given as follows:

$$\mathbf{Z} = \mathbf{h}(\mathbf{X}) + \boldsymbol{\nu} \tag{7}$$

where the column matrix of measurement function vector $\mathbf{h}(\mathbf{X})$ is written by

$$\mathbf{h}(\mathbf{X}) = \begin{bmatrix} \arctan 2(-z_{m1}, x_{m1}) \\ \arctan(y_{m1}/\sqrt{x_{m1}^2 + z_{m1}^2}) \\ \arctan 2(-z_{m2}, x_{m2}) \\ \arctan(y_{m2}/\sqrt{x_{m2}^2 + z_{m2}^2}) \\ \arctan 2(-z_{mb}, x_{mb}) \\ \arctan(y_{mb}/\sqrt{x_{mb}^2 + z_{mb}^2}) \\ \sqrt{x_{mb}^2 + y_{mb}^2 + z_{mb}^2} \end{bmatrix} \tag{8}$$

and $\boldsymbol{\nu}$ is the measurement noise vector. All measurement noises are assumed to be white Gaussian noises. We define the covariance matrix of measurement uncertainty $\mathbf{R}$ as

$$\begin{aligned} &E[\boldsymbol{\nu}(t)\boldsymbol{\nu}(t)^T] = \mathbf{R}\delta(t-\tau), \\ &\mathbf{R} = \mathrm{diag}([\sigma_{\alpha1}^2; \sigma_{\beta1}^2; \sigma_{\alpha2}^2; \sigma_{\beta2}^2; \sigma_{\alpha b}^2; \sigma_{\beta b}^2; \sigma_{\Delta r}^2]) \end{aligned} \tag{9}$$

where $\sigma_{\alpha1}$, $\sigma_{\beta1}$, $\sigma_{\alpha2}$, $\sigma_{\beta2}$, $\sigma_{\alpha b}$, $\sigma_{\beta b}$, and $\sigma_{\Delta r}$ are standard deviations of measurement noises. The covariance matrix of measurement uncertainty $\mathbf{R}$ is a 7×7 constant main diagonal matrix.

In Eq. (8), x_{m1}, y_{m1}, and z_{m1} are components of the vector $\Delta\mathbf{r}_1$ in the measurement frame of CCS; x_{m2}, y_{m2}, and z_{m2} are components of the vector $\Delta\mathbf{r}_2$ in the measurement frame of ACS; and x_{mb}, y_{mb}, and

Δz_{mb} are components of the vector $-\Delta\mathbf{r}_b$ in the measurement frame of ACS. They are written by

$$[\,x_{m1} \quad y_{m1} \quad z_{m1}\,]^T = L_{m1i} \cdot (\Delta\mathbf{r}_1)_i \tag{10}$$

$$[\,x_{m2} \quad y_{m2} \quad z_{m2}\,]^T = L_{m2i} \cdot [(\Delta\mathbf{r}_1)_i - (\Delta\mathbf{r}_b)_i] \tag{11}$$

$$[\,x_{mb} \quad y_{mb} \quad z_{mb}\,]^T = L_{m2i} \cdot (-\Delta\mathbf{r}_b)_i \tag{12}$$

where L_{m1i} is the transformation matrix from the inertial frame to the measurement frame of CCS, and L_{m2i} is the transformation matrix from the inertial frame to the measurement frame of ACS. They are the functions of inertial states and attitudes of spacecraft.

From the nonlinear process noise equation (5) and measurement equation (7), the discrete-time linearized equations about estimated values are obtained:

$$\delta\mathbf{X}_k = \mathbf{\Phi}_{k,k-1}\delta\mathbf{X}_{k-1} + B\mathbf{U}(t_{k-1}) + \mathbf{W}_{k-1} \tag{13}$$

$$\delta\mathbf{Z}_k = \mathbf{H}_k\delta\mathbf{X}_k + \mathbf{V}_{k-1} \tag{14}$$

where

$$\mathbf{\Phi}_{k,k-1} \approx \mathbf{I} + \Delta t \cdot \left.\frac{\partial\mathbf{f}(\mathbf{X})}{\partial\mathbf{X}}\right|_{\mathbf{X}=\hat{\mathbf{X}}_{k-1}}, \qquad \mathbf{H}_k = \left.\frac{\partial\mathbf{h}(\mathbf{X})}{\partial\mathbf{X}}\right|_{\mathbf{X}=\hat{\mathbf{X}}_k(-)}$$

$$\mathbf{W}_{k-1} = \int_{t_{k-1}}^{t_k} \mathbf{\Phi}_{t_k,\tau} D\varsigma(\tau)\, D\tau$$

Then the relative position and velocity of TS can be estimated precisely using discrete-time extended Kalman filter. The state estimation error covariance matrix is obtained as follows to analyze the observability of the navigation system:

$$\mathbf{K}_k = \mathbf{P}_{k/k-1}\mathbf{H}_k^T(\mathbf{H}_k\mathbf{P}_{k/k-1}\mathbf{H}_k^T + \mathbf{R}_k)^{-1} \tag{15}$$

$$\mathbf{P}_{k/k-1} = \mathbf{\Phi}_{k.k-1}\mathbf{P}_{k-1}\mathbf{\Phi}_{k,k-1}^T + \mathbf{Q}_{k-1} \tag{16}$$

$$\mathbf{P}_k = (\mathbf{I} - \mathbf{K}_k\mathbf{H}_k)\mathbf{P}_{k/k-1}(\mathbf{I} - \mathbf{K}_k\mathbf{H}_k)^T + \mathbf{K}_k\mathbf{R}_k\mathbf{K}_k^T \tag{17}$$

where $\mathbf{Q}$ is the covariance matrix of discrete-time process noise:

$$\mathbf{Q}_{k-1} = \int_{t_{k-1}}^{t_k} \mathbf{\Phi}_{t_k,\tau} D\mathbf{q} D^T \mathbf{\Phi}_{t_k,\tau}^T\, D\tau \tag{18}$$

The linearized matrices $\mathbf{\Phi}$ and $\mathbf{H}$ are evaluated with respect to the true nominal state values that are propagated using the nonlinear orbit models (Cowell's method [33]).

However, whether to determine the relative position of TS using geometry method or to estimate accurately the relative-motion states of TS via filter method, the triangle-measuring configuration is the necessary condition. As along as the separation angle between the LOS vector from CCS to TS and the LOS vector from ACS to TS γ is equal to zero or π, the triangle-measuring configuration disappears so that the double-LOS-measurement system degenerates into the single-LOS-measurement system. The results of analyzing the condition number of the observability matrix about the deterministic navigation system has also proved that the observability of the double-LOS-measuring relative navigation system becomes weak with the separation angle γ close to zero or π gradually [24]. Therefore, a path constraint (which is a keep-out cone with TS as the vertex and the connection line between TS and ACS as the centerline) must be taken into account in the course of rendezvous so as to prevent the separation angle being close to zero or π and to ensure a good observability of the relative navigation system (see Fig. 2). The path constraint is also expressed as follows:

$$1 - |\cos\gamma| > \varepsilon \tag{19}$$

where ε is a positive real number. The approach guidance maneuver of CCS for rendezvous with the target will be implemented under this path constraint.

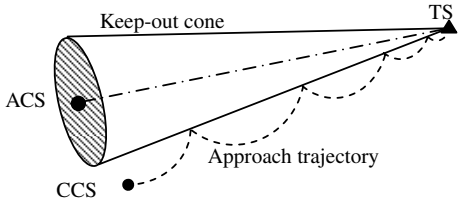

Fig. 2 Keep-out cone in the course of approach.

III. Approach Guidance with Navigation Constraint

Although double-LOS-measuring relative navigation method is useful to estimate the relative position and velocity of the target for noncooperative autonomous rendezvous, a path constraint arises from the observability of the navigation system. Therefore, the purpose of guidance is not only to direct CCS to the target with a controlled relative velocity, but to avoid CCS violating the path constraint. The use of artificial potential function guidance is useful in dealing with the problem of path-constrained rendezvous.

A. Attractive Potential and Repulsive Potential

To ensure convergence, the artificial potential guidance will be obtained according to Lyapunov's second method, which has the following conditions:

$$V(\mathbf{X}) > 0, \quad \forall\ \mathbf{X} \neq 0 \tag{20}$$

$$V(\mathbf{X}) = 0, \quad \text{as} \quad \mathbf{X} = 0, \quad \text{and} \quad V(\mathbf{X}) \to \infty, \quad \text{as} \quad \|\mathbf{X}\| \to \infty \tag{21}$$

$$\dot{V}(\mathbf{X}) < 0, \quad \forall\ \mathbf{X} \neq 0 \tag{22}$$

The potential function developed must have the property that there is a minimum at the goal position (attractive potential) and high regions of potential in the keep-out zone (repulsive potential). In this paper, we suppose that only CCS rendezvous with TS. Therefore, only the relative position variables of TS with respect to CCS are contained in the attractive potential. However, the keep-out cone caused by navigation constraint is related to the connection line between TS and ACS so that the repulsive potential includes the relative position variables of TS with respect to ACS. We define the relative position vector of TS with respect to CCS and ACS as

$$\mathbf{X}_1 = (\Delta\mathbf{r}_1)_i = [\,x_1 \quad y_1 \quad z_1\,]^T$$

$$\mathbf{X}_2 = (\Delta\mathbf{r}_2)_i = (\Delta\mathbf{r}_1)_i - (\Delta\mathbf{r}_b)_i = [\,x_2 \quad y_2 \quad z_2\,]^T$$

And the goal relative position of TS with respect to CCS is defined as

$$\mathbf{X}_1^g = (\Delta\mathbf{r}_1^g)_i = [\,x_1^g \quad y_1^g \quad z_1^g\,]^T$$

Then the attractive potential and the repulsive potential are given by

$$V_{\text{att}}(\mathbf{X}_1) = (\mathbf{X}_1 - \mathbf{X}_1^g)^T P(\mathbf{X}_1 - \mathbf{X}_1^g) \tag{23}$$

$$\begin{aligned} V_{\text{rep}}(\mathbf{X}_1, \mathbf{X}_2) &= \lambda(\mathbf{X}_1 - \mathbf{X}_1^g)^T P(\mathbf{X}_1 - \mathbf{X}_1^g)\exp\left[\frac{(\cos\gamma)^2}{\sigma}\right] \\ &= \lambda(\mathbf{X}_1 - \mathbf{X}_1^g)^T P(\mathbf{X}_1 - \mathbf{X}_1^g)\exp\left[\frac{(\mathbf{X}_1^T\mathbf{X}_2)^2}{\sigma\|\mathbf{X}_1\|^2\|\mathbf{X}_2\|^2}\right] \end{aligned} \tag{24}$$

where P is a positive definite matrix that is used with the attractive potential to give an ellipsoidal projection of the potential in the configuration space:

$$P = \mathrm{diag}([p_1, p_2, p_3]) \tag{25}$$

Parameters λ and σ, which are positive real numbers, determine the opening angle of the keep-out cone.

Obviously, the repulsive potential defined as Eq. (20) increases with the separation angle γ close to zero or π gradually and reaches a maximum as γ is equal to zero or π. It ensures that there is a high region of potential in the keep-out cone and the potential still has a unique minimum at $\mathbf{X}_1 = \mathbf{X}_1^g$. However, the relative position of TS with respect to ACS $\mathbf{X}_2$ is variable so that the keep-out cone defined by the repulsive-potential equation (24) is dynamic. The orientation of the keep-out cone in space changes with the direction of the relative position vector of TS with respect to ACS.

The total potential function is defined as the sum of the attractive and the repulsive potentials:

$$\begin{aligned} V(\mathbf{X}_1, \mathbf{X}_2) &= V_{\mathrm{att}}(\mathbf{X}_1) + V_{\mathrm{rep}}(\mathbf{X}_1, \mathbf{X}_2) \\ &= (\mathbf{X}_1 - \mathbf{X}_1^g)^T P(\mathbf{X}_1 - \mathbf{X}_1^g)\left(1 + \lambda \exp\left[\frac{(\mathbf{X}_1^T\mathbf{X}_2)^2}{\sigma\|\mathbf{X}_1\|^2\|\mathbf{X}_2\|^2}\right]\right) \end{aligned} \tag{26}$$

In this paper, only the convergence of the relative position of TS with respect to CCS $\mathbf{X}_1$ needs to be ensured. Therefore, the relative position $\mathbf{X}_1$ is taken as the state vector, but the relative position of TS with respect to ACS $\mathbf{X}_2$ is taken as the time-variable parameter in the potential function (26). Obviously, the following condition is guaranteed:

$$\lambda \exp[(\mathbf{X}_1^T\mathbf{X}_2)^2/(\sigma\|\mathbf{X}_1\|^2\|\mathbf{X}_2\|^2)] > 0, \quad \forall\ \mathbf{X}_1, \mathbf{X}_2$$

Therefore, the potential function (26) satisfies the first two conditions of Lyapunov's second method, Eqs. (20) and (21) for the relative position $\mathbf{X}_1$. Figure 3 shows a two-dimensional potential function with a keep-out cone under the assumption that $\mathbf{X}_2$ is constant [70 km, 0] and the goal relative position $\mathbf{X}_1^g$ is equal to zero. There are no singularities in the potential function.

B. Approach Guidance with Dynamic Keep-Out Cone

The approach guidance is designed according to the third condition of Lyapunov's second method. When the total derivative of the potential function is less than zero $\dot{V} < 0$, the motion of the chaser spacecraft is freely propagated. But, as long as $\dot{V} \geq 0$, an control impulse will be provided such that the relative velocity $\dot{\mathbf{X}}_1$ immediately is directly opposite to the partial derivative of the potential with respect to the state vector $\mathbf{X}_1$ after the impulse $\Delta\dot{\mathbf{X}}_1$:

$$\dot{\mathbf{X}}_1^* = \dot{\mathbf{X}}_1 + \Delta\dot{\mathbf{X}}_1 = -K\frac{\partial V(\mathbf{X}_1, \mathbf{X}_2)}{\partial \mathbf{X}_1} \tag{27}$$

where $\dot{\mathbf{X}}_1^*$ is the relative velocity after the control impulse. And K is a positive definite matrix:

$$K = \mathrm{diag}([k_1, k_2, k_3]) \tag{28}$$

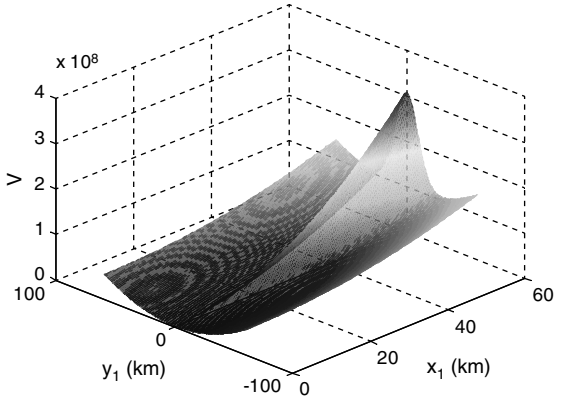

Fig. 3 Two-dimensional potential function with keep-out zone.

Since we suppose that CCS rendezvous with TS but ACS not, only CCS have control impulses. Using Eq. (27), three axes control impulses of CCS can be calculated as follows:

$$\Delta\dot{x}_1 = -\dot{x}_1 - k_1\frac{\partial V}{\partial x_1} \tag{29}$$

$$\Delta\dot{y}_1 = -\dot{y}_1 - k_2\frac{\partial V}{\partial y_1} \tag{30}$$

$$\Delta\dot{z}_1 = -\dot{z}_1 - k_2\frac{\partial V}{\partial z_1} \tag{31}$$

where

$$\begin{aligned} \frac{\partial V}{\partial x_1} &= 2p_1(x_1 - x_1^g)\left\{1 + \lambda\exp\left[\frac{(\mathbf{X}_1^T\mathbf{X}_2)^2}{\sigma\|\mathbf{X}_1\|^2\|\mathbf{X}_2\|^2}\right]\right\} \\ &\quad + (\mathbf{X}_1 - \mathbf{X}_1^g)^T P(\mathbf{X}_1 - \mathbf{X}_1^g) \\ &\quad \times \left\{\frac{2\lambda}{\sigma}\left[\frac{x_2\|\mathbf{X}_1\|^2(\mathbf{X}_1^T\mathbf{X}_2) - x_1(\mathbf{X}_1^T\mathbf{X}_2)^2}{\|\mathbf{X}_1\|^4\|\mathbf{X}_2\|^2}\right]\right. \\ &\quad \left.\times \exp\left[\frac{(\mathbf{X}_1^T\mathbf{X}_2)^2}{\sigma\|\mathbf{X}_1\|^2\|\mathbf{X}_2\|^2}\right]\right\} \end{aligned} \tag{32}$$

Table 1 Initial orbit elements of spacecraft

Orbit elements	TS	CCS	ACS
Semimajor axis a, M	7000000	6999700	6999900
Eccentricity e	0.002	0.0021	0.002
Orbit inclination i, deg	50.00	50.002	50.002
Right ascension node Ω, deg	10.00	10.002	10.002
Argument of perigee ω, deg	30.00	29.85	29.85
Mean anomaly M, deg	30.00	29.85	29.85

Table 2 Relative navigation parameters

Parameters	Value
Standard deviations of process acceleration noises	
$\sigma_{1x}, \sigma_{1y}, \sigma_{1z}$	0.01, m/s^2
$\sigma_{bx}, \sigma_{by}, \sigma_{bz}$	0.001, m/s^2
Standard deviations of measurement noises	
$\sigma_{\alpha 1}, \sigma_{\beta 1}$, deg	0.01, deg
$\sigma_{\alpha 2}, \sigma_{\beta 2}$, deg	0.01, deg
$\sigma_{\alpha b}, \sigma_{\beta b}$, deg	0.01, deg
$\sigma_{\Delta r}$m	5.0,
Standard deviations of inertial navigation errors	
Position, per axis	200, m
Velocity, per axis	1.0, m/s
Standard deviations of attitude determination errors	
Per axis	0.01, deg

Table 3 Approach guidance parameters

Parameters	Value
Goal relative position	[−200; 200; 200], m
Attractive potential	
p_1	0.022
p_2	0.022
p_3	0.022
Repulsive potential	
σ	0.05
λ	2.4e − 9
Control gain	
k_1	0.0083
k_2	0.0022
k_3	0.0002

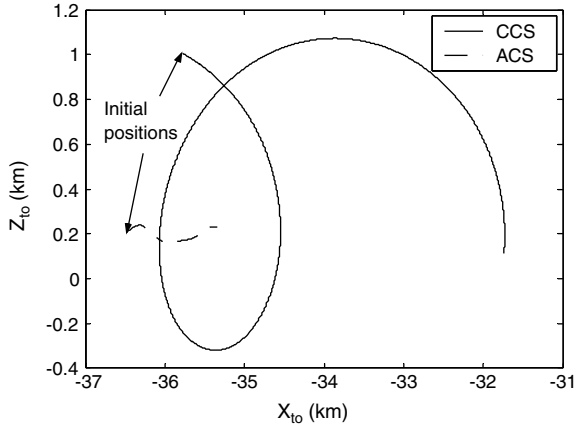

Fig. 4 Relative motions in TS orbit plane (without guidance).

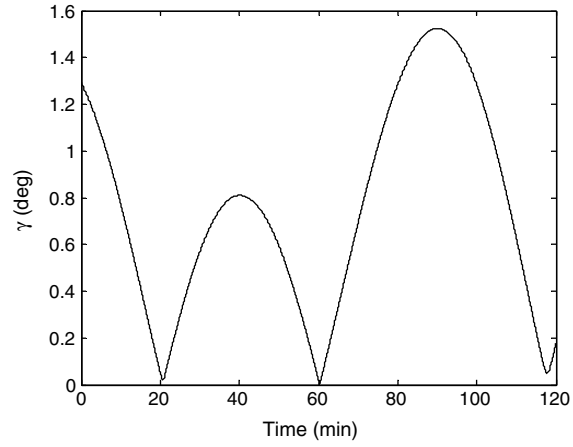

Fig. 5 Separation angle between two LOS vectors (without guidance).

$$\frac{\partial V}{\partial y_1} = 2p_2(y_1 - y_1^g)\left\{1 + \lambda \exp\left[\frac{(\mathbf{X}_1^T\mathbf{X}_2)^2}{\sigma\|\mathbf{X}_1\|^2\|\mathbf{X}_2\|^2}\right]\right\} + (\mathbf{X}_1 - \mathbf{X}_1^g)^T P(\mathbf{X}_1 - \mathbf{X}_1^g) \times \left\{\frac{2\lambda}{\sigma}\left[\frac{y_2\|\mathbf{X}_1\|^2(\mathbf{X}_1^T\mathbf{X}_2) - y_1(\mathbf{X}_1^T\mathbf{X}_2)^2}{\|\mathbf{X}_1\|^4\|\mathbf{X}_2\|^2}\right] \times \exp\left[\frac{(\mathbf{X}_1^T\mathbf{X}_2)^2}{\sigma\|\mathbf{X}_1\|^2\|\mathbf{X}_2\|^2}\right]\right\} \tag{33}$$

$$\frac{\partial V}{\partial z_1} = 2p_3(z_1 - z_1^g)\left\{1 + \lambda \exp\left[\frac{(\mathbf{X}_1^T\mathbf{X}_2)^2}{\sigma\|\mathbf{X}_1\|^2\|\mathbf{X}_2\|^2}\right]\right\} + (\mathbf{X}_1 - \mathbf{X}_1^g)^T P(\mathbf{X}_1 - \mathbf{X}_1^g) \times \left\{\frac{2\lambda}{\sigma}\left[\frac{z_2\|\mathbf{X}_1\|^2(\mathbf{X}_1^T\mathbf{X}_2) - z_1(\mathbf{X}_1^T\mathbf{X}_2)^2}{\|\mathbf{X}_1\|^4\|\mathbf{X}_2\|^2}\right] \times \exp\left[\frac{(\mathbf{X}_1^T\mathbf{X}_2)^2}{\sigma|\mathbf{X}_1|^2\|\mathbf{X}_2\|^2}\right]\right\} \tag{34}$$

The conditions given by Eqs. (29–31) define the control impulse magnitude and direction. After the impulse, the total derivative of the potential immediately is found to be

$$\dot{V} = \frac{\partial V}{\partial \mathbf{X}_1^T}\dot{\mathbf{X}}_1^* + \frac{\partial V}{\partial \mathbf{X}_2^T}\dot{\mathbf{X}}_2 = -\frac{\partial V}{\partial \mathbf{X}_1^T}K\frac{\partial V}{\partial \mathbf{X}_1} + \frac{\partial V}{\partial \mathbf{X}_2^T}\dot{\mathbf{X}}_2 \tag{35}$$

where

$$\frac{\partial V}{\partial \mathbf{X}_2^T} = \begin{bmatrix} \frac{\partial V}{\partial x_2} & \frac{\partial V}{\partial y_2} & \frac{\partial V}{\partial z_2} \end{bmatrix} \tag{36}$$

$$\frac{\partial V}{\partial x_2} = (\mathbf{X}_1 - \mathbf{X}_1^g)^T P(\mathbf{X}_1 - \mathbf{X}_1^g) \times \left\{\frac{2\lambda}{\sigma}\left[\frac{x_1\|\mathbf{X}_2\|^2(\mathbf{X}_1^T\mathbf{X}_2) - x_2(\mathbf{X}_1^T\mathbf{X}_2)^2}{\|\mathbf{X}_1\|^2\|\mathbf{X}_2\|^4}\right] \times \exp\left[\frac{(\mathbf{X}_1^T\mathbf{X}_2)^2}{\sigma\|\mathbf{X}_1\|^2\|\mathbf{X}_2\|^2}\right]\right\} \tag{37}$$

$$\frac{\partial V}{\partial y_2} = (\mathbf{X}_1 - \mathbf{X}_1^g)^T P(\mathbf{X}_1 - \mathbf{X}_1^g) \times \left\{\frac{2\lambda}{\sigma}\left[\frac{y_1\|\mathbf{X}_2\|^2(\mathbf{X}_1^T\mathbf{X}_2) - y_2(\mathbf{X}_1^T\mathbf{X}_2)^2}{\|\mathbf{X}_1\|^2\|\mathbf{X}_2\|^4}\right] \times \exp\left[\frac{(\mathbf{X}_1^T\mathbf{X}_2)^2}{\sigma\|\mathbf{X}_1\|^2\|\mathbf{X}_2\|^2}\right]\right\} \tag{38}$$

$$\frac{\partial V}{\partial z_2} = (\mathbf{X}_1 - \mathbf{X}_1^g)^T P(\mathbf{X}_1 - \mathbf{X}_1^g) \times \left\{\frac{2\lambda}{\sigma}\left[\frac{z_1\|\mathbf{X}_2\|^2(\mathbf{X}_1^T\mathbf{X}_2) - z_2(\mathbf{X}_1^T\mathbf{X}_2)^2}{\|\mathbf{X}_1\|^2\|\mathbf{X}_2\|^4}\right] \times \exp\left[\frac{(\mathbf{X}_1^T\mathbf{X}_2)^2 w}{\sigma\|\mathbf{X}_1\|^2\|\mathbf{X}_2\|^2}\right]\right\} \tag{39}$$

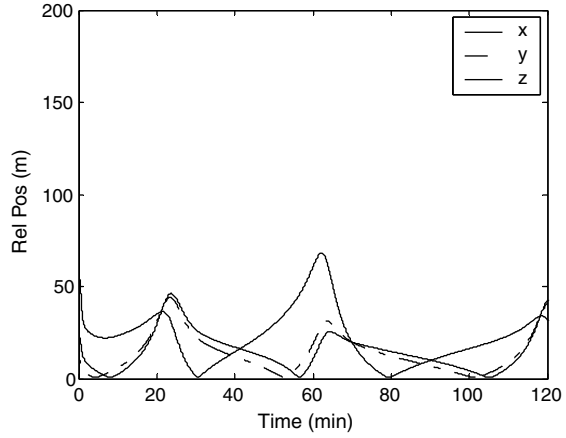

a) Square roots of the relative position covariance

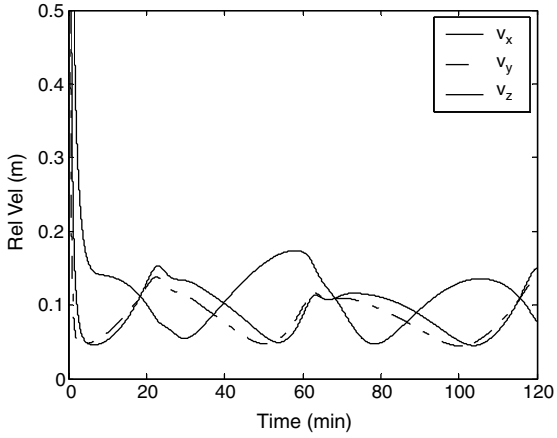

b) Square roots of the relative velocity covariance

Fig. 6 Error covariance propagations of the relative position and velocity of TS with respect to CCS (without guidance).

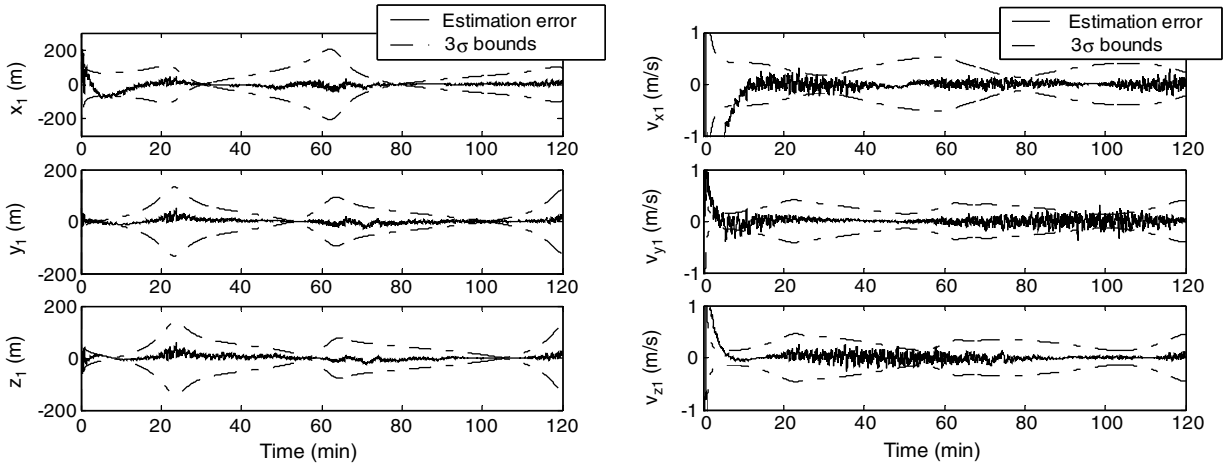

a) Relative position estimation error b) Relative velocity estimation error

Fig. 7 Estimation errors of the relative motion of TS with respect to CCS in the inertial frame and corresponding 3σ bounds (without guidance).

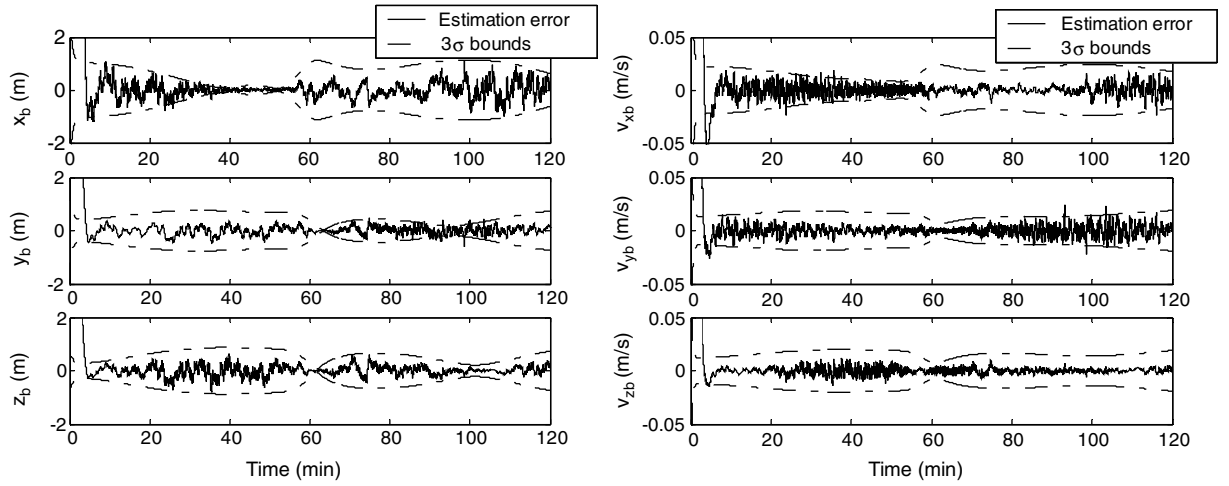

a) Relative position estimation error b) Relative velocity estimation error

Fig. 8 Estimation errors of the relative motion of ACS with respect to CCS in the inertial frame and corresponding 3σ bounds (without guidance).

In Eq. (27), the total derivative of the potential contains the partial derivative of the potential with respect to the relative position $\mathbf{X}_2$ because the keep-out cone defined by the repulsive potential (24) is dynamic. Therefore, it is difficult to ensure $\dot{V} < 0$ in any case. But in this paper, we suppose that ACS and TS have not orbital control such that the relative position $\mathbf{X}_2$ and relative velocity $\dot{\mathbf{X}}_2$ of TS with respect to ACS are all bounded. Meanwhile, the following conditions are established in the course of approach:

$$\frac{\partial V}{\partial \mathbf{X}_1^T} \cdot \frac{\partial V}{\partial \mathbf{X}_1} > 0, \quad \text{as} \quad \mathbf{X}_1 \neq \mathbf{X}_1^g \tag{40}$$

$$\left\| \frac{\partial V}{\partial \mathbf{X}_1^T} \cdot \frac{\partial V}{\partial \mathbf{X}_1} \right\| \gg \left\| \frac{\partial V}{\partial \mathbf{X}_2} \right\|, \quad \text{as} \quad \mathbf{X}_1 \neq \mathbf{X}_1^g \tag{41}$$

Therefore, there exists a positive number ξ to make

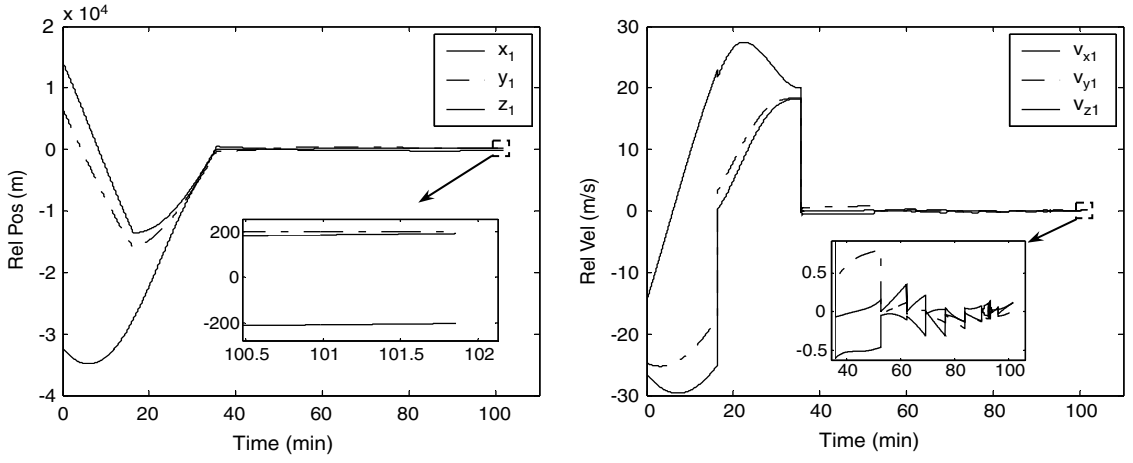

Fig. 9 Relative position and velocity of TS with respect to CCS (guidance with keep-out zone).

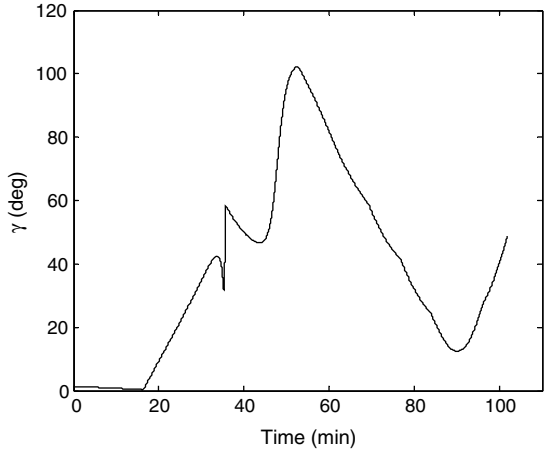

Fig. 10 Separation angle between two LOS vectors (guidance with keep-out zone).

$$\left|\frac{\partial V}{\partial \mathbf{X}_2^T}\dot{\mathbf{X}}_2\right| \Big/ \left(\frac{\partial V}{\partial \mathbf{X}_1^T}\cdot\frac{\partial V}{\partial \mathbf{X}_1}\right) < \xi \tag{42}$$

Furthermore, we define the minimum of the elements of control gain matrix as $k_m = \min(k_1, k_2, k_3)$. As long as choosing $k_m > \xi$, the total derivative of the potential is then found to be

$$\begin{aligned}\dot{V} &= -\frac{\partial V}{\partial \mathbf{X}_1^T}K\frac{\partial V}{\partial \mathbf{X}_1} + \frac{\partial V}{\partial \mathbf{X}_2^T}\dot{\mathbf{X}}_2 \le -k_m\left(\frac{\partial V}{\partial \mathbf{X}_1^T}\cdot\frac{\partial V}{\partial \mathbf{X}_1}\right) + \frac{\partial V}{\partial \mathbf{X}_2^T}\dot{\mathbf{X}}_2 \\ &< -\xi\left(\frac{\partial V}{\partial \mathbf{X}_1^T}\cdot\frac{\partial V}{\partial \mathbf{X}_1}\right) + \left|\frac{\partial V}{\partial \mathbf{X}_2^T}\dot{\mathbf{X}}_2\right| < 0\end{aligned} \tag{43}$$

Since the total derivative of the potential is now negative definite, global asymptotic convergence is ensured. Meanwhile, according to Eqs. (32–34), the partial derivatives of the potential with respect to the state vector $\mathbf{X}_1$ converge to zero as long as the convergence of the state vector $\mathbf{X}_1$ is ensured:

$$\frac{\partial V}{\partial x_1} \to 0, \qquad \frac{\partial V}{\partial y_1} \to 0, \qquad \frac{\partial V}{\partial z_1} \to 0, \quad \text{as} \quad \|\mathbf{X}_1 - \mathbf{X}_1^g\| \to 0$$

Therefore, the convergence of the relative velocity $\dot{\mathbf{X}}_1$ is also ensured by Eq. (27):

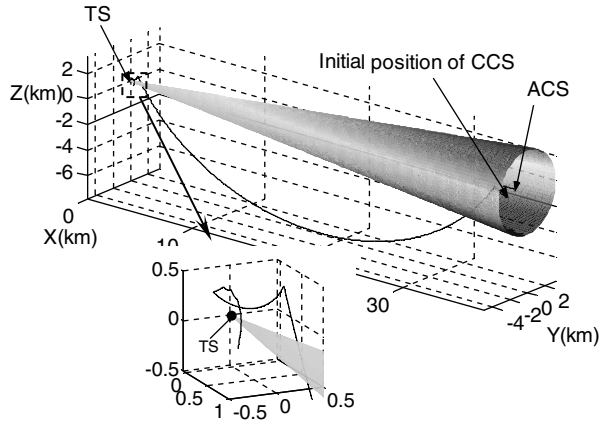

Fig. 12 Relative motions in 3-D space (guidance with keep-out zone).

$$\|\dot{\mathbf{X}}_1\| = \sqrt{\left(k_1\frac{\partial V}{\partial x_1}\right)^2 + \left(k_2\frac{\partial V}{\partial y_1}\right)^2 + \left(k_3\frac{\partial V}{\partial z_1}\right)^2} \to 0, \quad \text{as} \quad \|\mathbf{X}_1 - \mathbf{X}_1^g\| \to 0 \tag{44}$$

The control impulses for approach guidance can be summarized as follows:

$$\mathbf{U}_{c1} = \begin{cases} 0, & \text{if } \dot{V} < 0, \\ \left(-\dot{\mathbf{X}}_1 - K\frac{\partial V}{\partial \mathbf{X}_1}\right)\delta(t), & \text{if } \dot{V} \ge 0 \end{cases} \tag{45}$$

where δ denotes the Dirac delta operator. The times and total number of control impulses are determined by the total derivative of the potential $\dot{V}$ autonomously. And the magnitudes and directions of control impulses are determined by the relative velocity of TS with respect to CCS and the partial derivative of the potential with respect to the state vector $\mathbf{X}_1$.

IV. Numerical Simulations and Analysis

To illustrate the presented approach guidance, we undertake two numerical simulation scenarios. In the first scenario, three spacecraft are freely propagated without any orbital control. But in the second scenario, the approach guidance of CCS is performed.

The initial classical orbit elements of spacecraft are given in Table 1. Using the initial orbit elements, we can calculate the initial inertial positions and velocities of spacecraft, which are taken as the initial values for numerical integration. And then, using a standard

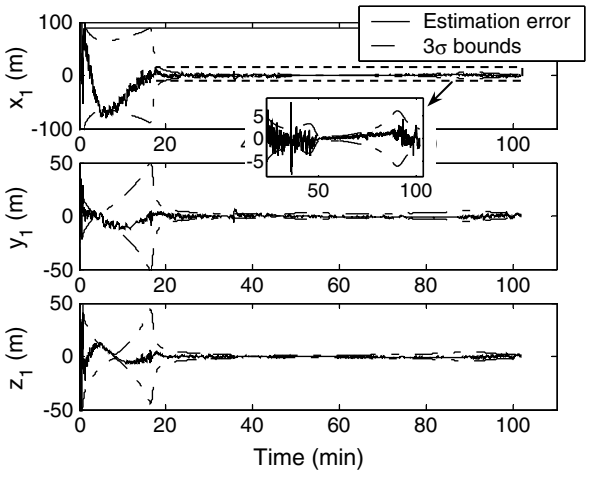

a) Relative position estimation error

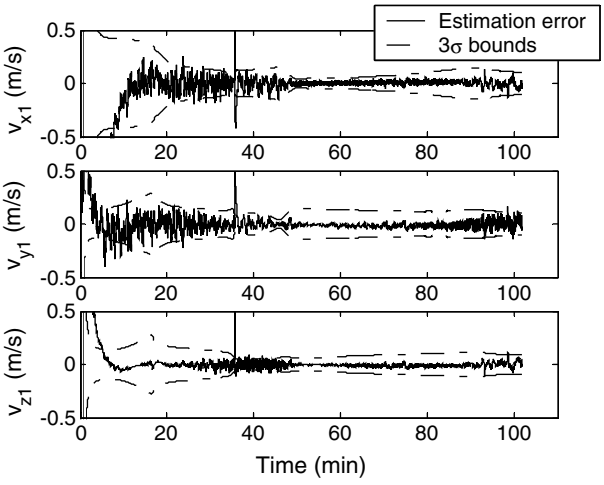

b) Relative velocity estimation error

Fig. 11 Estimation errors of the relative motion of TS with respect to CCS in the inertial frame and corresponding 3σ bounds (guidance with keep-out zone).

fourth-order Runge–Kutta method with a fixed step of 0.2 s, the numerical simulations are performed by integrating the nonlinear orbit equations (Cowell's method). The orbital perturbation accelerations include the gravitational zonal J_2 through J_4 effects. All simulations are carried out with MATLAB version 6.5 M files and Simulink models.

The process acceleration noises, measurement noises and the other interrelated errors are given in Table 2. The initial estimation of state vector is given by

$$\hat{\mathbf{X}}_0 = [-30\ \text{km};\quad 10\ \text{km};\quad 10\ \text{km};\quad 0;\quad 0;\quad 0;\quad 5\ \text{km};\quad 2\ \text{km};\quad 2\ \text{km};\quad 0;\quad 0;\quad 0]^T$$

And the initial covariance matrix is given by

$$\mathbf{P}_0 = \text{diag}\{[(1\ \text{km})^2;\ (1\ \text{km})^2;\ (1\ \text{km})^2;\ (5\ \text{m/s})^2;\ (5\ \text{m/s})^2;\ (5\ \text{m/s})^2;\ (50\ \text{m})^2;\ (50\ \text{m})^2;\ (50\ \text{m})^2;\ (1\ \text{m/s})^2;\ (1\ \text{m/s})^2;\ (1\ \text{m/s})^2]\}$$

The approach guidance parameters are given in Table 3.

A. Scenario 1: Numerical Simulation Without Approach Guidance

According to initial orbit elements of spacecraft, CCS and ACS lag behind TS more than 36 km in along-track motion at first (see Fig. 4). Figure 5 shows that the separation angle between LOS vector from CCS to TS and LOS vector from ACS to TS γ is close to zero 3 times in a 120 min simulation. Figure 6 shows that the square roots of error covariances of the relative position and velocity of TS with respect to CCS are convergent rapidly although there are large initial error covariances. But the error covariances increase with the separation angle γ close to zero. Especially, the square root of error covariance of the relative position reaches to nearly 70 m as the separation angle γ decreases to 0.0023 deg in the vicinity of the 60th minute. The results indicate that the observability of double-LOS-measuring relative navigation system becomes weak with the separation angle γ close to zero gradually. Therefore, it is necessary for the relative navigation to prevent three spacecraft being in one line.

The results of relative states estimation using double-LOS-measuring relative navigation method without approach guidance control are also shown in Figs. 7 and 8. The estimation error of the relative position of TS with respect to CCS per axis can converge to the accuracy of less than 20 m and the relative velocity estimation error per axis can converge to the accuracy of less than 0.2 m/s (see Fig. 7). Moreover, the estimation errors of the relative states of TS also increase with the separation angle γ close to zero because of the poor observability of the navigation system in those situations. The estimation error of the relative position of ACS with respect to CCS per axis can converge to the accuracy of less than 2 m and the relative velocity estimation error per axis can converge to the accuracy of less than 0.02 m/s (see Fig. 8). The estimation errors of the relative motion of ACS with respect to CCS are one order of magnitude less than those of TS with respect to CCS because there are the relative range measurements between ACS and CCS via interspacecraft crosslink, but not between TS and CCS.

B. Scenario 2: Numerical Simulation with Approach Guidance

In this simulation scenario, the approach guidance control is started after a 5 min simulation and the simulation is stopped until CCS reaches the goal position within 10 m.

The results for the approach guidance with the keep-out zone constraint are given in Figs. 9–14. Figure 9 shows that it takes CCS about 102 min to reach the goal position. Finally, the relative velocity of TS with respect to CCS converges to less than 0.1 m/s. Figure 10 shows that the separation angle between two LOS vectors is small in the beginning of simulation, and after the approach guidance starts, it increases fast and is guaranteed to be a larger value all along. Therefore, the good observability of the relative navigation system is ensured and the estimations of the relative position and velocity become more accurate. Figure 11 shows that the estimation error of the relative position of TS with respect to CCS per axis can converge to the accuracy of less than 5 m, and the relative velocity estimation error per axis can converge to the accuracy of less than 0.1 m/s. The three-dimensional relative motions of CCS and ACS are shown in Fig. 12, where the frame origin is located at the center of mass of TS and the X axis points ACS all along. The keep-out cone with a 10 deg opening angle is also shown in Fig. 12. CCS is in the keep-out cone at first and than moves out the keep-out cone under the effect of the approach guidance control. Figure 13 shows the guidance control impulses in three axes. Twenty-one time impulses and a total Δv of

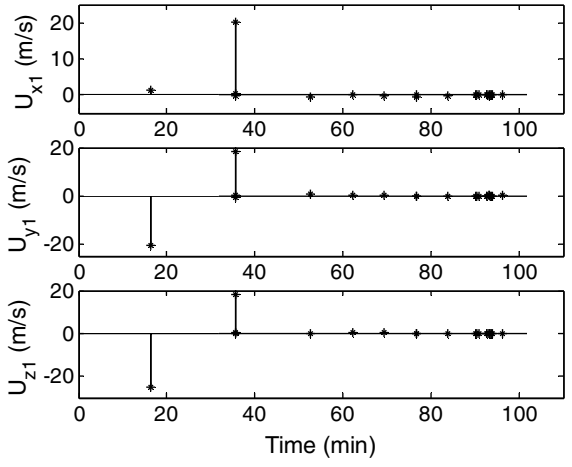

Fig. 13 Guidance control impulses in three axes (guidance with keep-out zone).

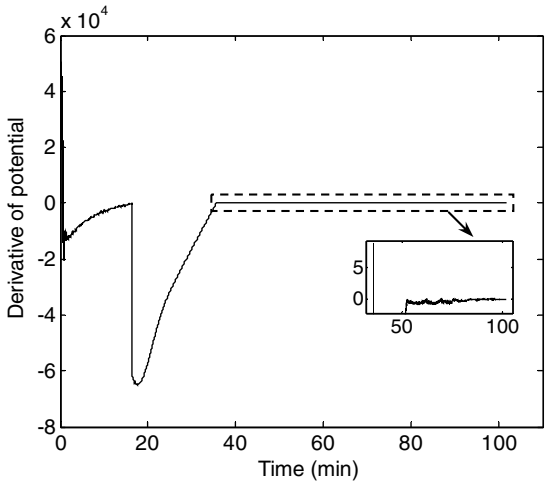

Fig. 14 Total derivative of potential (guidance with keep-out zone).

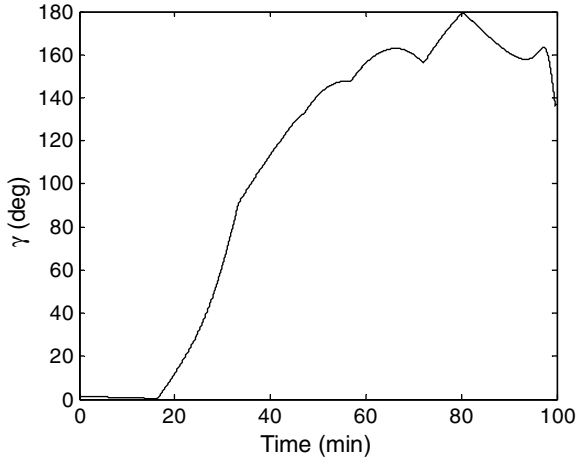

Fig. 15 Separation angle between two LOS vectors (guidance without keep-out zone).

111.62 m/s are required to bring CCS to within 10 m of the goal position. Every impulse occurs as the total derivative of potential is larger than zero (see Fig. 14).

In this simulation, the first impulse occurs at the 983.8th second and requires 47.12 m/s Δv. The second impulse occurs at the 2137.6th second and requires 56.94 m/s. The time interval between the two impulses is only 1153.8 s, but CCS has been close to within several hundreds meters of the target after the two impulses. C-W two-impulse rendezvous guidance is also calculated to compare with the approach guidance method presented. The initial relative states in local-vertical/local-horizontal (LVLH) frame are calculated according to the initial classical orbit elements of spacecraft given in Table 1 and the final relative states in LVLH frame is given as [0;0;0;0;0;0]. The transfer time is set as 1150 s. The total Δv required by C-W two-impulse rendezvous guidance is 92.37 m/s. Obviously, C-W two-impulse rendezvous guidance requires less Δv than the approach guidance method presented. However, C-W rendezvous guidance is based on the linearized relative-motion equations with the assumptions of small eccentricity and near relative distance and is merely an open loop guidance method. Therefore, C-W two-impulse rendezvous guidance will cause large guidance error in the real nonlinear orbit model. It always requires additional midcourse correction Δv to rendezvous with the target accurately.

For comparing with the above results, the approach guidance without the keep-out zone constraint is also simulated. In this simulation, λ is set as 0 to totally remove the repulsive potential, but all the other guidance parameters in Table 3 are still used. Figure 15 shows that the separation angle between LOS vector from CCS to TS and LOS vector from ACS to TS γ is close to π in the vicinity of the 80th minute because of removing the keep-out zone constraint. Figure 16 shows that CCS flies ahead of TS and passes through the keep-out cone under the effect of the approach guidance. Figure 17 shows that the estimation errors of the relative states of TS increase in the vicinity of the 80th minute. The results illuminate that the observability of the navigation system cannot be ensured if the keep-out zone constraint is removed in the approach guidance.

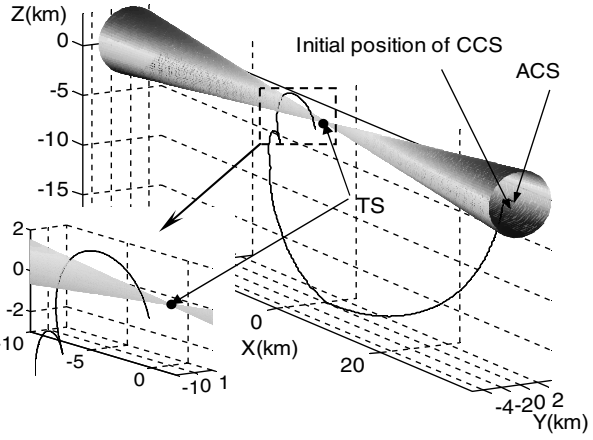

Fig. 16 Relative motions in 3-D space (guidance without keep-out zone).

V. Conclusions

Although double-LOS-measuring relative navigation is useful to estimate the relative position and relative velocity of the autonomous rendezvous target, the triangle-measuring constraint must be taken into account in the course of approach and rendezvous. Via analyzing the state estimation error covariance, it is proved again that the degree of observability of double-LOS-measuring navigation system is weak as the separation angle γ between two LOS vector is close to zero or π. Therefore, a relative-motion path constraint, which is a keep-out cone with TS as the vertex and the connection line between TS and ACS as the centerline, is set up. And then, an approach guidance law with the navigation constraint for autonomous rendezvous is designed using artificial potential function method. It is ensured that there is a high region of potential in the keep-out cone and the potential still has a unique minimum at the goal position. The results of numerical simulations illustrate that the guidance law not only ensures CCS to reach the goal position for rendezvous, but also prevents CCS from entering the keep-out cone.

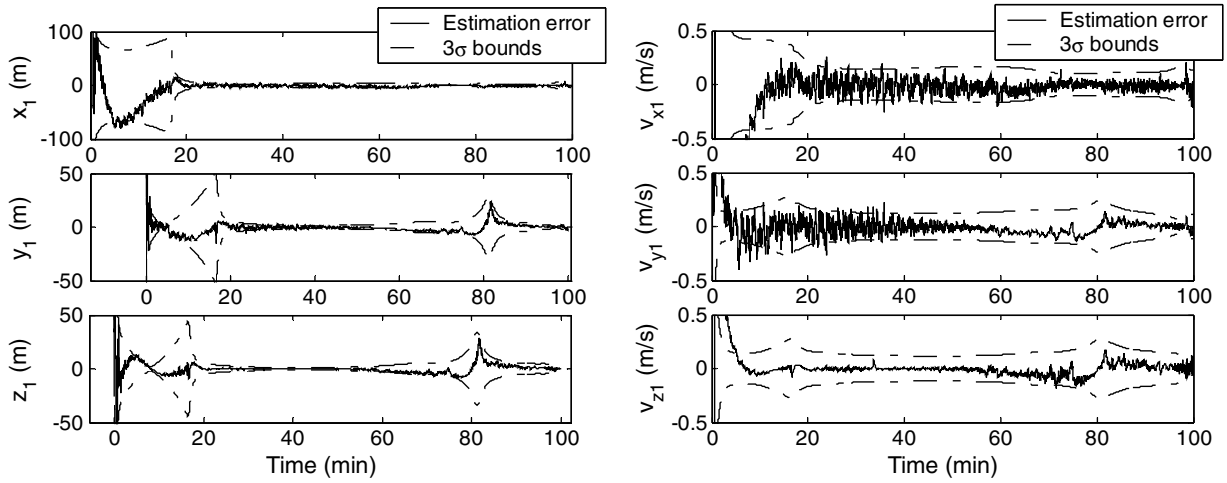

Fig. 17 Estimation errors of the relative motion of TS with respect to CCS in the inertial frame and corresponding 3σ bounds (guidance without keep-out zone).

The presented angles-only guidance method could be adopted in some autonomous rendezvous mission comprising several chase spacecraft, especially the far- or medium-range approach operation. Because only LOS-angle measurements of the target are required, the chase spacecraft need merely to equip the simple vision measuring sensors. This is the prominent advantage of the presented guidance method.

Acknowledgments

The paper is supported by the National Natural Science Foundation of China (ref. 10802002). The authors thank the Associate Editor and the reviewers for their helpful suggestion and revision to improve this paper.

References

[1] Zimpfer, D., Kachmar, P., and Tuohy, S., "Autonomous Rendezvous, Capture and In-Space Assembly: Past, Present and Future," AIAA Paper 2005-2523, 2005.

[2] Mulder, T. A., "Orbital Express Autonomous Rendezvous and Capture Flight Operations—Part 1: Mission Description, AR&C Exercises 1, 2 and 3," AAS Paper 08-209, 2008.

[3] Baize, L., and Novelli, A., "ATV "Jules Verne" Control Centre, from Challenges to Success," AIAA Paper 2010-2124, 2010.

[4] Debus, T. J., and Dougherty, S. P., "Overview and Performance of the Front-End Robotics Enabling Near-Term Demonstration (FREND) Robotic Arm," AIAA Paper 2009-1870, 2009.

[5] Frauenholz, R. B., Bhat, R. S., Chesley, S. R., Mastrodemos, N., Owen, W. M., Jr., and Ryne, M. S., "Deep Impact Navigation System Performance," *Journal of Spacecraft and Rockets*, Vol. 45, No. 1, 2008, pp. 39–56.
doi:10.2514/1.24310

[6] Sherwood, B., "Mars Sample Return: Architecture and Mission Design," *Acta Astronautica*, Vol. 53, 2003, pp. 353–364.
doi:10.1016/S0094-5765(03)00153-X

[7] Polites, M. E., "An Assessment of the Technology of Automated Rendezvous and Capture in Space," NASA TP1998-208528, 1998.

[8] Woffinden, D. C., and Geller, D. K., "Navigating the Road to Autonomous Orbital Rendezvous," *Journal of Spacecraft and Rockets*, Vol. 44, No. 4, 2007, pp. 898–908.
doi:10.2514/1.30734

[9] Grimson W. E. L., "Computational Experiments with a Feature Based Stereo Algorithm," *IEEE Transactions on Pattern Analysis and Machine Intelligence*, Vol. PAMI-7, No. 1, 1985, pp. 17–34.
doi:10.1109/TPAMI.1985.4767615

[10] Cavanagh, P., "Reconstructing the Third Dimension: Interactions between Color, Texture, Motion, Binocular Disparity, and Shape," *Computer Vision, Graphics, and Image Processing*, Vol. 37, 1987, pp. 171–195.
doi:10.1016/S0734-189X(87)80001-4

[11] Masaki, I., "Three Dimensional Vision System for Intelligent Vehicles," *Industrial Electronics, Control, and Instrumentation (IECON'93)*, Vol. 3, 1993, pp. 1712–1717.

[12] Crassidis, J. L., Alonso, R., and Junkins, J. L., "Optimal Attitude and Position Determination from Line-of-Sight Measurements," *Journal of the Astronautical Sciences*, Vol. 48, Nos. 2–3, 2000, pp. 391–408.

[13] Woffinden, D. C., "Angles-Only Navigation for Autonomous Orbital Rendezvous," Ph.D. Dissertation, Utah State University, Logan, UT, 2008.

[14] Woffinden, D. C., and Geller, D. K., "Relative Angles-Only Navigation and Pose Estimation for Autonomous Orbital Rendezvous," *Journal of Guidance, Control, and Dynamics*, Vol. 30, No. 5, 2007, pp. 1455–1469.
doi:10.2514/1.28216

[15] Kim, S., Crassidis, J. L., Cheng, Y., and Fosbury, A. M., "Kalman Filtering for Relative Spacecraft Attitude and Position Estimation," *Journal of Guidance, Control, and Dynamics*, Vol. 30, No. 1, 2007, pp. 133–143.
doi:10.2514/1.22377

[16] Chari R. J. V., "Autonomous Orbital Rendezvous Using Angles-Only Navigation," Master Dissertation, Massachusetts Institute of Technology, Cambridge, MA, 2001.

[17] Yim, J. R., Crassidis, J. L., and Junkins, J. L., "Autonomous Orbit Navigation of Two Spacecraft System using Relative Line of Sight Vector Measurements," AAS Paper 04-257, 2004.

[18] Woffinden, D. C., and Geller, D. K., "Observability Criteria for Angles-Only Navigation," AAS Paper 07-402, 2007.

[19] Hablani, H. B., Tapper, M. L., and Dana-Bashian, D. J., "Guidance and Relative Navigation for Autonomous Rendezvous in A Circular Orbit," *Journal of Guidance, Control, and Dynamics*, Vol. 25, No. 3, 2002, pp. 553–562.
doi:10.2514/2.4916

[20] Hablani, H. B., "Autonomous Relative Navigation, Attitude Determination, Pointing and Tracking for Spacecraft Rendezvous," AIAA Paper 2003-5355, 2003.

[21] Hablani, H. B., "Autonomous Inertial Relative Navigation with Sight-Line-Stabilized Integrated Sensors for Spacecraft Rendezvous," *Journal of Guidance, Control, and Dynamics*, Vol. 32, No. 1, 2009, pp. 172–183.
doi:10.2514/1.36559

[22] Chen, T., Xu, S., and Wang, S., "Relative Motion Control for Autonomous Rendezvous Based on Classical Orbit Element Differences," *Journal of Guidance, Control, and Dynamics*, Vol. 30, No. 4, 2007, pp. 1003–1014.
doi:10.2514/1.28250

[23] Schmidt, J., and Lovell, T. A., "Estimating Geometric Aspects of Relative Satellite Motion Using Angles-Only Measurements," AIAA Paper 2008-6604, 2008.

[24] Chen, T., and Xu, S., "Double Line-of-Sight Measuring Relative Navigation for Spacecraft Autonomous Rendezvous," *Acta Astronautica*, Vol. 67, Nos. 1–2, 2010, pp. 122–134.
doi:10.1016/j.actaastro.2009.12.010

[25] Linares, R., Crassidis, J. L., and Cheng, Y., "Constrained Relative Attitude Determination for Two Vehicle Formations," AIAA Paper 2009-5882, 2009.

[26] Clohessy, W. H., and Wilshire, R. S., "Terminal Guidance System for Satellite Rendezvous," *Journal of the Aerospace Sciences*, Vol. 27, No. 9, 1960, pp. 653–658, 674.

[27] Vallado, D., and McClain, W., *Fundamentals of Astrodynamics and Applications*, 3rd ed., Microcosm, Hawthorne, CA, 2007, Chap. 6.

[28] Prussing, J. E., "Optimal Two- and Three-Impulse Fixed-Time Rendezvous in the Vicinity of a Circular Orbit," *AIAA Journal*, Vol. 8, No. 7, 1970, pp. 1221–1228.
doi:10.2514/3.5876

[29] Carter, T., "Fuel-Optimal Maneuvers of a Spacecraft Relative to a Point in Circular Orbit," *Journal of Guidance, Control, and Dynamics*, Vol. 7, No. 6, 1984, pp. 710–716.
doi:10.2514/3.19917

[30] Schaub, H., and Alfriend, K. T., "Impulsive Feedback Control to Establish Specific Mean Orbit Elements of Spacecraft Formations," *Journal of Guidance, Control, and Dynamics*, Vol. 24, No. 4, 2001, pp. 739–745.
doi:10.2514/2.4774

[31] Lopez, I., and McInnes, C. R., "Autonomous Rendezvous Using Artificial Potential Function Guidance," *Journal of Guidance, Control, and Dynamics*, Vol. 18, No. 2, 1995, pp. 237–241.
doi:10.2514/3.21375

[32] Yamanaka, K., and Ankersen, F., "New State Transition Matrix for Relative Motion on an Arbitrary Elliptical Orbit," *Journal of Guidance, Control, and Dynamics*, Vol. 25, No. 1, 2002, pp. 60–66.
doi:10.2514/2.4875

[33] Battin, R. H., *An Introduction to the Mathematics and Methods of Astrodynamics*, AIAA Education Series, AIAA, New York, 1987, pp. 206–212, 447, 498.